

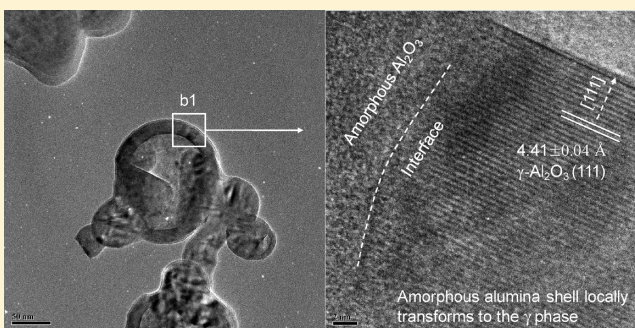
Microstructural Behavior of the Alumina Shell and Aluminum Core Before and After Melting of Aluminum Nanoparticles

Dudi Adi Firmansyah,[†] Kyle Sullivan,[‡] Kwang-Sung Lee,[†] Yong Ho Kim,[†] Riyan Zahaf,[†] Michael R. Zachariah,^{*,‡} and Donggeun Lee^{*,†}

[†]School of Mechanical Engineering, Pusan Clean Coal Center, Pusan National University, Busan 609-735, South Korea

[‡]Department of Mechanical Engineering and Department of Chemistry and Biochemistry, University of Maryland, Maryland 20742, United States

ABSTRACT: The oxidation mechanism of nanoaluminum particles, nominally employed as fuel component, is still an unsettled problem, because of the complex nature of thermo-mechanical properties of the oxide shell surrounding the elemental core. Although mechanical breakage of the alumina shell upon or after melting of aluminum core has been thought to play a key role in the combustion of aluminum nanoparticles, there has been little direct evidence. In this study, the microstructural behaviors of Al core and alumina shell lattices were investigated with increasing temperatures. Three in situ techniques, high-temperature X-ray diffraction analysis, hot-stage transmission electron microscopy, and high-resolution transmission electron microscopy for heat-treated samples, were employed to probe the thermal behaviors of aluminum and alumina lattices before and after melting of the aluminum core. High-temperature X-ray diffraction analysis revealed that nano aluminum lattice was initially expanded under tension at room temperature, and then when heated passed through a zero-strain state at ~ 300 °C. Upon further heating above the bulk melting temperature of aluminum, the aluminum lattice expanded under almost no constraint. This interesting observation, which is contrary to almost all of the previous results and models, was ascribed to the inhomogeneous (localized) crystalline phase transformation of amorphous alumina. High-resolution transmission electron microscopy and in situ hot-stage transmission electron microscopy evidenced localized phase transformation accompanied by a significant shell thickening, presumably resulting from diffusion processes of Al cations and O anions, which is to absorb the pressure built in aluminum core, by creating a more ductile shell.



1. INTRODUCTION

Aluminum (Al) nanoparticles have attracted an intense interest over the years as reactive additives in formulations of explosives and propellants,¹ as well as components of nanocomposite thermite materials,² mostly because of their higher and faster energy release (in some cases by several orders of magnitude) as compared to micrometer-sized Al particles.³ Thus, these promising prospects have triggered many studies: (1) to find reaction characteristics^{4,5} of aluminum nanoparticles such as the ignition temperature and delay, and (2) to understand a key mechanism^{6–13} for the enhanced reactivity. Experimental results consistently find that the ignition of nanosized aluminum occurs well below the ignition temperature of micrometer-sized (10–100 μm) particles, and close to the melting temperature of aluminum.⁶ One point, therefore, which is widely agreed upon is that understanding the interaction between the low melting aluminum core (660 °C) and high melting aluminum oxide shell (2054 °C) is a necessary prerequisite to understanding the ignition and combustion mechanism of nanosized aluminum.^{9–13}

According to a mechanism suggested by Trunov et al.,^{6,7} Al nanoparticles, normally coated with thin aluminum oxide shell, oxidize in several consecutive processes with increasing temperatures:

growth of amorphous oxide shell, amorphous-to- γ phase transformation, growth of γ alumina, γ -to- α phase transformation, and growth of α alumina. Among those steps, the “amorphous-to- γ phase transformation” was suggested as a key process for the stepwise increase in reactivity around the onset temperature of Al melting. Park et al.⁸ reported size-dependent oxidation kinetics of single Al nanoparticle during isothermal heating, which was characterized by “species diffusions” of Al and/or oxygen through the oxide shell.

On the other hand, Levitas et al.^{10–13} argued that for the diffusion coefficient of the species in the order of 10^{-18} – 10^{-19} $\text{cm}^2 \text{s}^{-1}$, the diffusion time required for the species to penetrate 2 nm-thick α alumina shell was almost 10 orders of magnitude longer than the conventional reaction time⁹ of ~ 10 – 100 μs . Thus, they proposed a new mechanism named “melt dispersion mechanism” that requires no breakage until complete melting of the Al core and thereby sufficiently high pressure buildup in the molten Al. Those requirements are likely fulfilled for fast heating (10^6 – 10^8 K/s)

Received: October 3, 2011

Revised: December 11, 2011

Published: December 13, 2011

and small relative radius of Al core ($M = R/\delta$ where R is Al core radius and δ is the thickness of the oxide shell). Despite their plausible explanation, there is no direct experimental evidence for explosive rupture of the oxide shell and the ejection of tiny molten Al clusters.

Recently, Chowdhury et al.⁹ conducted ignition experiments by fast heating Al/CuO thermite (Al particles of ~ 23 nm in radius with ~ 2 nm thick Al_2O_3 shell mixed with CuO nanopowders of ~ 100 nm) at the rate of $\sim 10^6$ K/s using a hot wire. They found that effective diffusion coefficient (D_{eff}) estimated from the measured ignition delay time was in the order of 10^{-10} $\text{cm}^2 \text{s}^{-1}$, 8–9 orders of magnitude larger than the typical value of species diffusion coefficient, suggesting that the species diffusion could govern the reaction. Henz et al.¹⁴ reported that built-in electric fields promoted ionic movement in the oxide shell, thus greatly enhancing the effective diffusion coefficient. These recent results suggest that a diffusion-based mechanism is a realistic possibility. Despite these results, there is still debate as to the ignition mechanism, and one factor affecting this is the unclear knowledge of the microstructural behavior of the Al_2O_3 shell before and after melting of Al core.

Using high-temperature X-ray diffraction (HT-XRD), Mei et al.¹⁵ reported that an Al core of $R = 40$ nm coated with 5 nm-thick amorphous Al_2O_3 shell began to melt at ~ 10 °C below the bulk melting temperature ($T_{\text{m,b}} = 660$ °C), and the melting of Al ended at ~ 659 °C. In contrast, when the original sample was heat-treated to produce smaller Al cores with thicker oxide shells ($R = 20$ nm, $\delta = 20$ nm), the heat-treated sample was superheated to 7–15 °C beyond $T_{\text{m,b}}$. The superheating was attributed to compressive pressure buildup in the Al core under the constraint of the thickened oxide shell. This is likely contrary to Sun and Simon's observation¹⁶ that the Al melting temperature (T_{m}) decreases from 656 to 647 °C when decreasing Al particle radius from 46 nm ($\delta = 4.2$ nm) to 11 nm ($\delta = 5.3$ nm). Levitas et al.¹³ argued that the inconsistent observation in T_{m} resulted from the fact that the different definitions of T_{m} were used when using HT-XRD and differential scanning calorimetry. They also showed that the T_{m} when defined as an initiation temperature of melting became reduced with decreasing core Al size. On the other hand, Rufino et al.¹⁷ reported there were no apparent differences in aluminum lattice expansion and T_{m} between nano- and micrometer samples unless the oxide shell was as thick as ~ 20 nm. This gives rise to a very surprising conclusion that an Al core of $R = 100$ nm expands as much as bulk Al does, and the 3 nm-thick amorphous shell is too thin to generate any compressive strain in the Al core, even though the oxide shell undergoes crystalline phase transformation. This has never been expected by any existing mechanisms.^{6,7,10–13}

The objectives of this research are therefore to elucidate the thermal behaviors of crystalline lattices of an Al core and Al_2O_3 shell, and to observe microstructural changes in the shell lattice, before and after Al melting. An in situ measurement of HT-XRD was conducted up to 800 °C for the first objective. Hot-stage transmission electron microscopy (HT-TEM) was used for tracing the overall morphological change of the sample with heating, and a high-resolution TEM on the heat-treated sample was employed for the second objective.

2. EXPERIMENTAL SECTION

A commercial aluminum powder provided from Argonide Co. has been used in this study and is designated as “100 nm Alex” by the supplier. TEM image analysis reveals that the

particles have a count mean outer diameter of ~ 96 nm with oxide thickness of ~ 2 nm. To remove any existing organic pollutants, the pristine sample was heated to 380 °C at 10 °C min^{-1} under air flow of 90 $\text{cm}^3 \text{min}^{-1}$ and then maintained at that temperature for 10 min. High-resolution transmission electron micrograph (HR-TEM) of the sample was obtained by operating JEM 3010 (JEOL) at 300 kV with a Gatan digital camera MSC-794. Figure 1a shows that the heat-treated Alex particle is coated with a 4.3 nm-thick Al_2O_3 shell. Figure 1a also clearly shows that the oxide shell still remains amorphous after the heat treatment. The inset of Figure 1 shows that the Alex particles are almost spherical and lightly aggregated. Figure 1b and c shows distributions of outer diameter and shell thickness of the particles. During the heat treatment, the oxide shell was thickened from ~ 2 nm for the pristine particles, decreasing the active Al content from 83.6 to 68.0 wt %. Dynamic thermogravimetric analysis (TGA, TA Instrument) was also conducted for the sample in air with increasing temperature up to 1300 at 10 °C min^{-1} . Given the initial sample mass of 5.45 mg, the total mass gain at 1300 °C was 4.85 mg. Provided the stoichiometric oxidation of aluminum, on the basis of the mass increase, an initial mass fraction of Al at 25 °C (that is the active Al content) was 62.9 wt %, fairly consistent with that given from the TEM analysis.

Two in situ techniques, high-temperature X-ray diffraction (HT-XRD) and hot-stage TEM, were employed in an effort to heat particles, and simultaneously monitor intrinsic behavior of atomic lattices, and overall shapes of the particles, respectively. HT-XRD profiles were obtained under vacuum ($\sim 10^{-2}$ Torr) with a commercial instrument (Rigaku, D/MAX-2500 18 kW) equipped with a vertical goniometer, and a multipurpose high-temperature attachment. When the sample was heated to a user-specified temperature (between 25 and 800 °C) at the rate of 10 °C min^{-1} , the XRD profile was recorded in the range of 26° – 70° in 2θ unit at 10°min^{-1} with irradiation of Cu $K\alpha$ X-ray (30 kV, 40 mA, 0.15405 nm). During the XRD measurement, the sample temperature was kept constant, and then increased for the next-temperature measurement. A standard Si polycrystal has been used for calibration of peak position. Hot-stage TEM experiments were also conducted under high vacuum ($\sim 10^{-6}$ Torr) on a JEM 2100 Lab6 TEM (JEOL) microscope at 200 kV and with a Gatan digital camera (Orius 1000). TEM images of the particles were taken in situ at the elevated temperatures. Unfortunately, thermal vibration at high temperatures as well as the low coherence of the Lab6 gun of the microscope results in a strong attenuation of the contrast transfer function at high spatial frequencies, making high-resolution images nearly impossible. To get around this limitation, each sample was heated at different temperatures under Ar flow in the TGA machine. The sample was then quenched to room temperature and dispersed in ethanol. The suspension was then violently stirred in an ultrasonic bath for 5 min. A few drops of the suspension were micro-pipetted to a carbon-coated copper grid, and then dried at room temperature for further HR-TEM imaging.^{18–21}

3. RESULTS AND DISCUSSION

3.1. Melting of the Al Core and Phase Transformation of Alumina Shell. Figure 2 shows XRD profiles taken in situ at elevated temperatures. At room temperature, three major peaks appear at $2\theta = 38.4^\circ$, 44.6° , and 65.0° , corresponding to (111), (200), and (220) reflections of metallic aluminum, respectively.

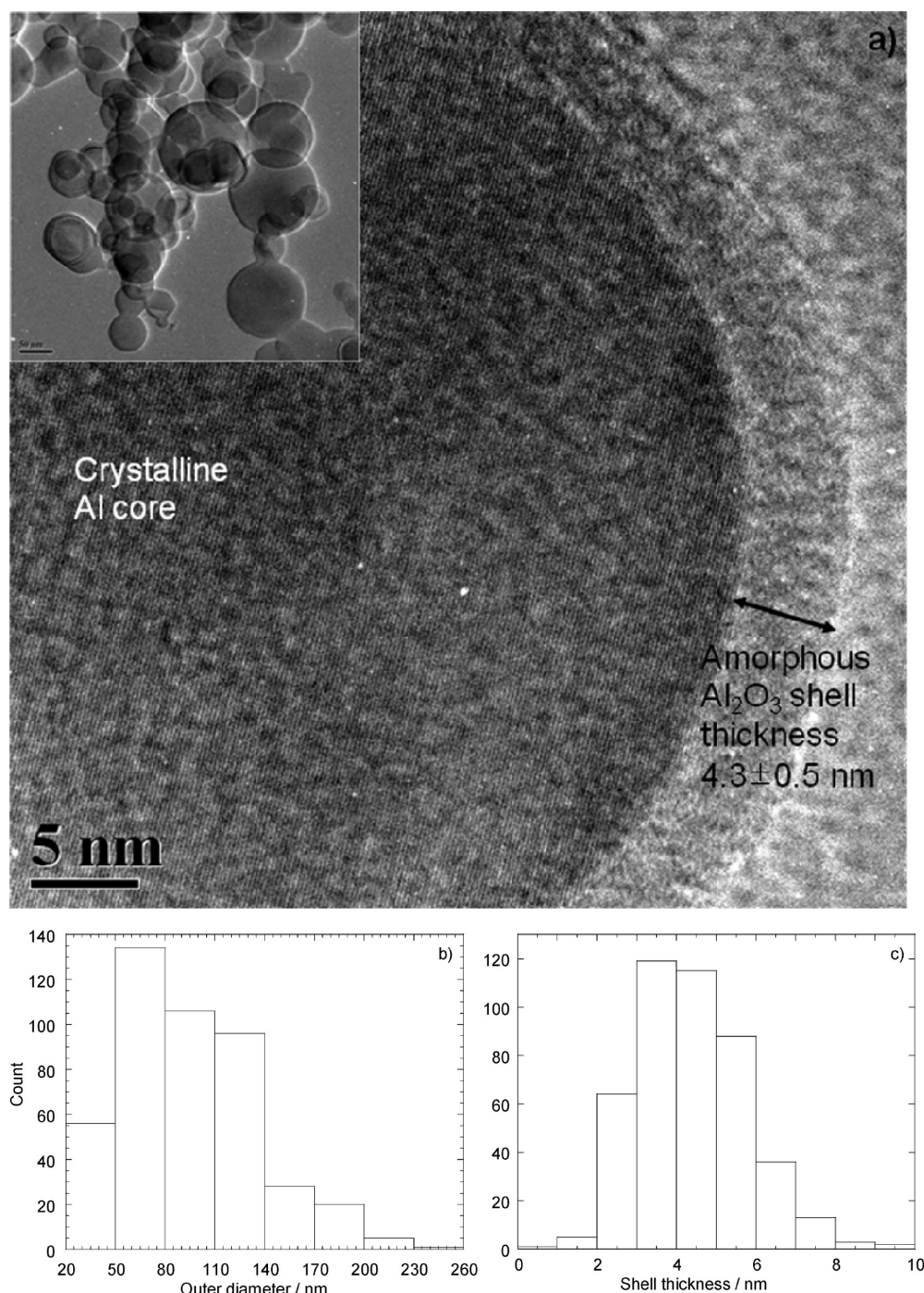


Figure 1. Size and morphology of Alex nanoaluminum particles: (a) HR-TEM image, (b) size distribution of aluminum core, and (c) size distribution of alumina shell thickness; the total counts are 445.

The peak positions are in good agreement with the JCPDS file (no. 040787). The absence of any crystalline alumina peaks indicates that the alumina shell is mainly amorphous as seen in Figure 1. As sample temperature increases over 300 °C, the intensities of the three Al peaks markedly decrease, and eventually disappear above 690 °C, indicating that some of the Al core may be melting between 300 and 600 °C, and keeps melting until 690 °C.

In the work of Mei et al.,¹⁵ Al melting began at ~647 °C, and the Al core (60 nm diameter), which has an at least 13 nm-thick

alumina shell, was superheated to 7–15 °C above the bulk melting temperature (660 °C). The super heating was attributed to compressive pressure buildup in the Al core. Using differential scanning calorimetry (DSC), Trunov et al.⁷ reported for 44–121 nm-sized particles that the onset temperature of Al melting was lowered to 590 °C. In contrast, Rufino et al.¹⁷ showed no apparent effects of particle size (200 vs 8100 nm) and the nature of the shell (oxide or organics) on melting temperature; all powders showed almost identical endothermic DSC peaks around 660 °C (see Figure 2 in ref 17). It is notable that XRD peaks decrease

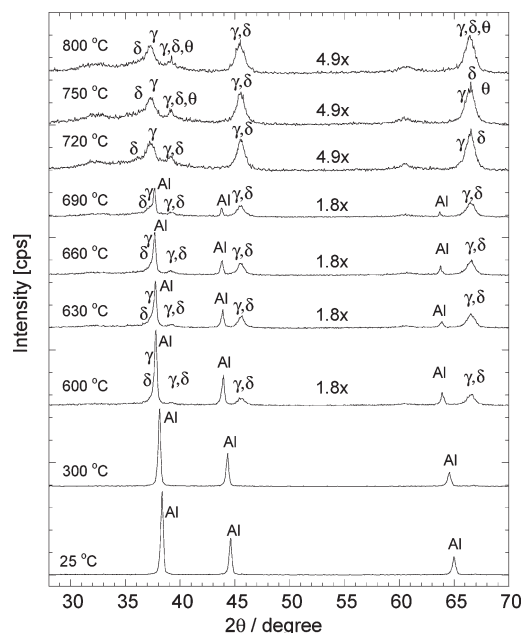


Figure 2. High-temperature X-ray diffraction patterns of Alex nanoparticles in situ obtained at various temperatures. The values of $1.8\times$ and $4.9\times$ are the magnification scale from the original intensity.

slightly with increasing temperature due to thermal scattering of X-ray even before significant melting occurs.¹⁵ A similar peak decrease was also observed with temperature ramping up to 500 °C during in situ XRD measurement (see Figure 5 of Rufino et al.¹⁷). Thus, it is still an ongoing issue to determine the initiation temperature of aluminum.

Figure 2 also shows that the amorphous alumina begins to transform to γ and δ phases at 600 °C and the crystallization becomes more pronounced at higher temperatures. Above 750 °C, the θ phase of alumina begins to develop. As noted in the figure, many peaks of the γ and δ phases are apparently overlapped presumably due to the proximity of their densities.⁶ This makes it harder to separate the hidden peaks of alumina polymorphs, as compared to relatively distinct Al peaks. This is the reason that the thermal behavior of the alumina lattice has rarely been evidenced in a quantitative manner.

To circumvent this, a commercial software (PEAKFIT v4, SPSS Inc.) was combined with a user defined function (UDF) that can incorporate peak information of the JCPDS files for the existing polymorphs; for example, a group of peaks of a single crystalline phase, maintaining relative peak intensities, was allowed to vary in the vicinity of peak positions predicted by the JCPDS and linear expansion coefficients. Included for the fitting is every major peak with a relative intensity larger than 25% of the biggest peak of each phase from the JCPDS files (no. 100425 for γ alumina;²² no. 160394 for δ alumina;²³ no. 231009 for θ alumina²³). It was reported that there are some variations in the fitted data of peak intensity and position even when repeating a generic fitting process for the same experimental data.²⁴ To enhance the reliability of the fitting, three independent fittings were conducted for each XRD profile, and then the resultant standard deviation for each peak was provided to the UDF, as a constraint limiting the range of subpeak shift during the final fitting.

Figure 3 shows how this fitting method works for the XRD data at 690 °C. As seen in the figure, the experimental data

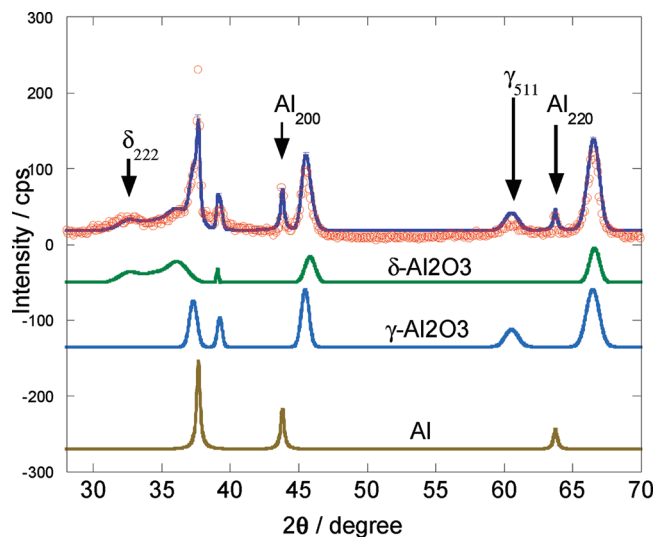


Figure 3. A deconvolution peak analysis of the X-ray diffraction pattern at 690 °C. Error bars represent the uncertainty calculated from the standard deviation of three independent fittings.

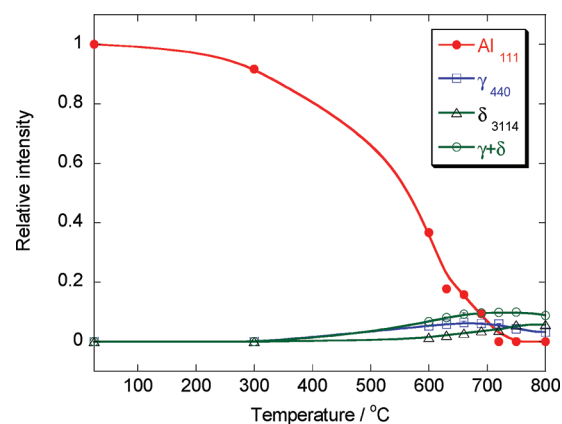


Figure 4. Thermal behaviors of aluminum core and the three crystalline phases of alumina shell with increasing temperature. Error bars represent the uncertainty of intensity calculated from the standard deviation of three independent fittings.

denoted by circles are reasonably well fitted by the solid line that is the sum of the simulated XRD profiles of the Al and two phases of alumina. As previously mentioned, the peak intensities for each phase, when they are normalized by the biggest value, are in good agreement with the JCPDS data. Another thing to be noted is that there exist some markers, which can be used as reference data for quantitative evaluation of each phase, as marked with arrows in the figure. In other words, the (200) or (220) peak of Al, the (222) peak of δ alumina, and the (511) peak of γ alumina are separated clearly from the surrounding peaks of other phases, which allows the reasonable prediction of the biggest peak intensity of each phase on the basis of the markers.

In this way, the XRD profiles in Figure 2 are all quantitatively analyzed to give the necessary information, that is, the intensities and positions of the peaks. As the peak intensity is an indicator of the abundance of each phase,²⁵ the biggest peak intensities of the Al and two phases of alumina, after being normalized by the

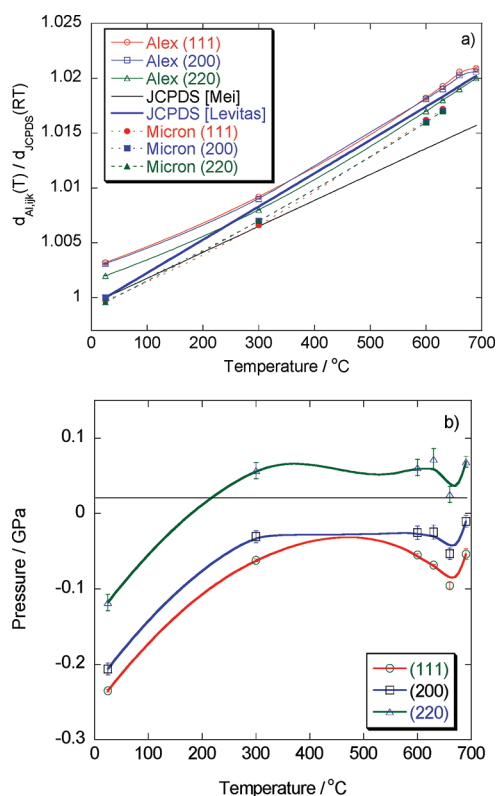


Figure 5. (a) Lattice expansions of aluminum nanoparticles as a function of temperature in comparison with micrometer-sized aluminum particles. (b) Resultant pressure built in the aluminum core. Error bars represent the uncertainty of lattice thermal expansion and pressure calculated from the standard deviation of three independent fittings. The lines are shown for a guide by smoothing the data points.

intensity of Al (111) peak at room temperature, are plotted against the temperature to describe the melting of Al and phase transformation of alumina. Figure 4 indicates that the sum of the relative intensities of γ and δ phases, as a measure of molar ratio of crystalline alumina to aluminum, increases with increasing temperature and reaches $\sim 10\%$ of the initial concentration of aluminum. Given the radius of Al core (48 nm) and thickness of alumina shell (4.3 nm) from TEM image analysis, the initial molar ratio of amorphous alumina to aluminum is estimated to be 9.9%, very close to the value from Figure 4.

3.2. Thermal Behaviors of Atomic Lattices of the Al Core and Al_2O_3 Shell. It is generally accepted that the Al lattice expansion is constrained by a less expanding alumina shell so that the compressive pressure is built up in the Al core, resulting in a tensile stress in the alumina shell that might result in shell breakage. Of particular interest is therefore to monitor variations of lattice spacings (d_{hkl}) of the Al core and alumina shell with increasing temperature. Interestingly, Figure 2 again shows that the Al peak positions (θ_{hkl}) keep moving toward lower 2θ angles with increasing temperature, which is indicative of thermal expansion of the Al lattice.¹⁵ Given the relationship of $d_{hkl} = \lambda/2 \sin \theta_{hkl}$ (where $\lambda = 0.154$ nm), the lattice spacings of the three crystallographic planes of the Al ($d_{hkl,\text{Al}}$) are estimated from the peak positions measured at various temperatures. The same HT-XRD analysis has been conducted for a micrometer-sized Al powder (Aldrich, >97%) in which any size-related effects are expected to be negligible.

Figure 5a compares the thermal variations of the three Al lattice spacings of the Alex and micrometer samples normalized by the corresponding values from JCPDS at room temperature. At room temperature, the Alex powder initially has an expanded lattice structure, as compared to the micrometer sample whose lattice spacings are in good agreements with JCPDS. Given the JCPDS values of lattice spacings at room temperature d_{JCPDS} (25 °C), the lattice expansion of bulk aluminum under no constraint might be predicted as a function of temperature by using the linear expansion coefficient α as $d_{\text{JCPDS}}(T) = d_{\text{JCPDS}}(25 \text{ °C}) [1 + \alpha(T - 25 \text{ °C})]$, which would be referred to as “JCPDS indication” and is shown as a linear line in Figure 5a. Note that two different values have been used for the α of the bulk Al ($2.36 \times 10^{-5} \text{ K}^{-1}$ from Mei et al.¹⁵ vs $3.03 \times 10^{-5} \text{ K}^{-1}$ from Levitas et al.¹³). Hence, the corresponding two linear lines are shown in the figure. Interestingly, the relative lattice spacings of the micrometer sample lie safely between the two JCPDS indications. The three sets of lattice spacings of micrometer sample are very close to each other, suggesting that the micrometer sample undergoes an isotropic thermal expansion under no constraints. In contrast, the lattice of the Alex sample is apparently under mild expansion.

On the basis of the lattice spacings of Alex sample, the pressure buildup in the Al core is estimated by $P = K_{\text{Al}}[d_{\text{JCPDS}}(T) - d_{\text{ijk}}(T)]/d_{\text{JCPDS}}(T)$, where K_{Al} is the bulk modulus of Al (71.1–76 GPa)^{13,15} and $d_{\text{ijk}}(T)$ is the experimental data measured by the HT-XRD at elevated temperatures T . Figure 5b shows the thermal variations of the pressure buildup of the Alex nano powder. It is noted that the calculation was made on the basis of the α from Levitas et al.¹³ When increasing the temperature to 300 °C, the initial negative pressure, representing a kind of “tension” forcing the lattice expansion, seems to be relieved although the data are relatively scattered. A possible explanation of this would be as follows. Provided the alumina forming temperature (T_{ox}) around 300 °C as seen in Figure 5b, the less shrinking alumina shell hinders the Al core from contracting during cooling after its formation, which results in lattice expansions in both the shell and the core at room temperature. When the sample is heated again to the T_{ox} , any lattice strain is relieved, and the resultant pressure is zeroed.

A question then arises as to why, when the temperature increases from 300 °C to the Al melting temperature, the pressure is zeroed where positive (compressive) pressure buildup is expected due to the less expanding shell. The experiment in Figure 5a shows almost no compression in the Al core lattice even for the upper limit of the JCPDS indication (using the higher value of α), suggesting that the Al core undergoes a free thermal expansion with no constraint above 300 °C. This is impossible unless the shell is flexible enough to relieve any compressive strain in the Al core. Such a flexible nature of the shell has never been reported except Rufino et al.¹⁷ who reported that there is no difference in lattice expansion behaviors of nano- and micrometer-sized Al particles when increasing temperatures to 630 °C.

It is noted that above 300 °C, the amorphous phase that is believed most flexible begins to transform to the denser γ phase. If the phase transformation occurs homogeneously, the harder γ -phase shell must compress the expanding core at least at the time of a complete phase transformation. Thus, no compression of the Al core suggests the opposite case, that is, an inhomogeneous phase transformation in which the remaining amorphous region or amorphous– γ interface may offer a sort of localized

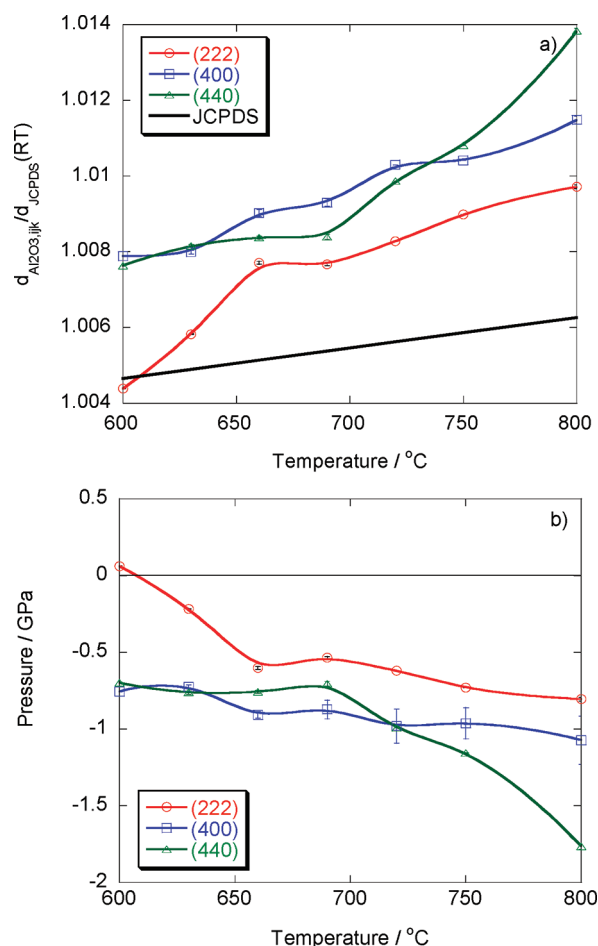


Figure 6. (a) Lattice expansions of (b) resultant pressure built in the alumina shell as a function of temperature. Error bars represent the uncertainty calculated from the standard deviation of three independent fittings. The lines are shown for a guide by smoothing the data points.

buffer space to absorb the compressive pressure. This speculation will be discussed in the next section. Likewise, a similar analysis has been conducted for the alumina lattice. Figure 6a and b shows the thermal variations of the alumina lattice spacings and the resultant pressure buildup in the alumina shell. Recall that the relative lattice spacings in Figure 6a are obtained by normalizing the measured values of lattice spacing with the corresponding values from the JCPDS at 25 °C. The solid line in Figure 6a stands for the JCPDS indication estimated by taking the mean value of the α of the alumina between $8.4 \times 10^{-6} \text{ K}^{-1}$ of Mei et al.¹⁵ and $7.78 \times 10^{-6} \text{ K}^{-1}$ of Levitas et al.¹³ Interestingly, the alumina shell expands along the major crystallographic directions such as [222], [400], and [440], in such a way that the negative pressure increases with ramping temperature.

3.3. HR-TEM Observation of the Lattice of the Alumina Shell Before and After Melting of Al Core. To date, no doubt has arisen on the “conventional wisdom” that any lattice events such as expansion, crystalline phase transformation, breakage, and/or oxidative growth occur homogeneously or randomly throughout the shell and the core. Although this sort of hypothesis has been a basis for model developments and data interpretations, it is now contrary to our speculation in the previous section: the localized inhomogeneous phase transformation. As the amorphous-to-crystalline transformation is apparently complete

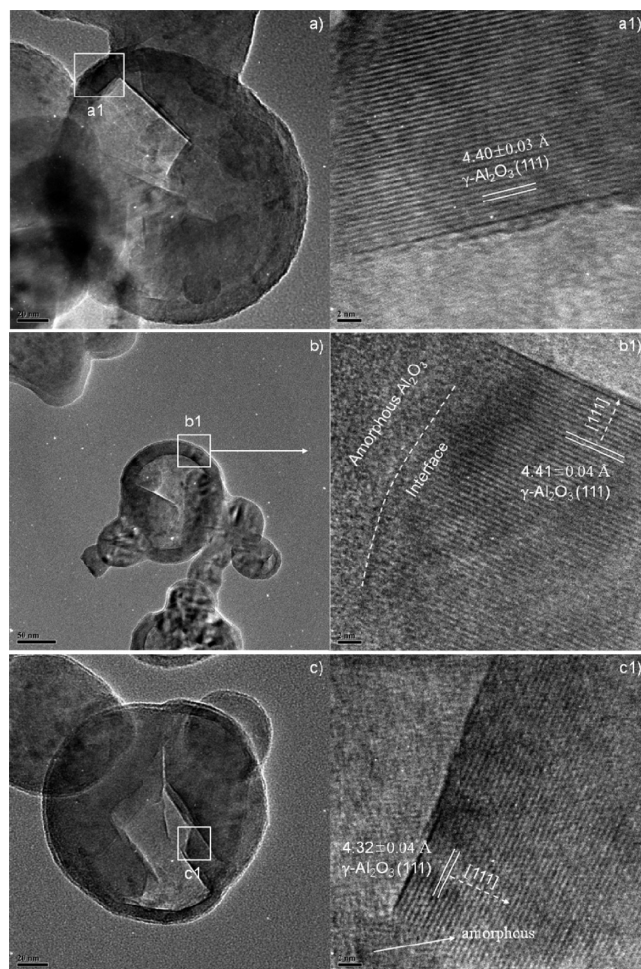


Figure 7. HR-TEM images of aluminum nanoparticles obtained at 660 °C. Insets of low-magnification (a)–(c) as indicated with boxes are shown on the right.

above 660 °C (see the plateau of $\gamma+\delta$ profile in Figure 4), the Alex powder was heated to 660 °C in Ar gas, then cooled to room temperature, and then observed using HR-TEM in an attempt to evidence how the phase transformation occurs and how the shell is broken. Figure 7a–c and their magnified images (Figure 7a1–c1) indicate three interesting things: (1) the alumina shell is thickened from 4.3 to ~ 10 nm even in the absence of nominal oxygen source (Ar flow), (2) the shell fractures with sharp edges, which are well crystallized to γ phase, and (3) the initial shell is inhomogeneously (locally) crystallized as indicated in Figure 7b1.

The shell thickening even in the absence of oxygen might be evidence of diffusive migration of Al atoms/cations through the alumina shell,^{14,26} which has never been demonstrated by experiment. Using molecular dynamics simulations, Henz et al.¹⁴ concluded that the outward diffusion of Al with the help of the built-in electric field is mainly responsible for the enhanced ignition mechanism of aluminum nanoparticles and results in apparent thickening of the alumina shell. It is notable that these interstitial Al atoms in the alumina lattice very likely expand the oxide lattice, which would be pronounced more with increasing temperatures.¹⁴ This is exactly consistent with the observations in Figure 6. Second, the sharp fractured surface of the γ phase in the absence of major lattice bending in Figure 7 might be an indicator that there existed several weak points (believed near the

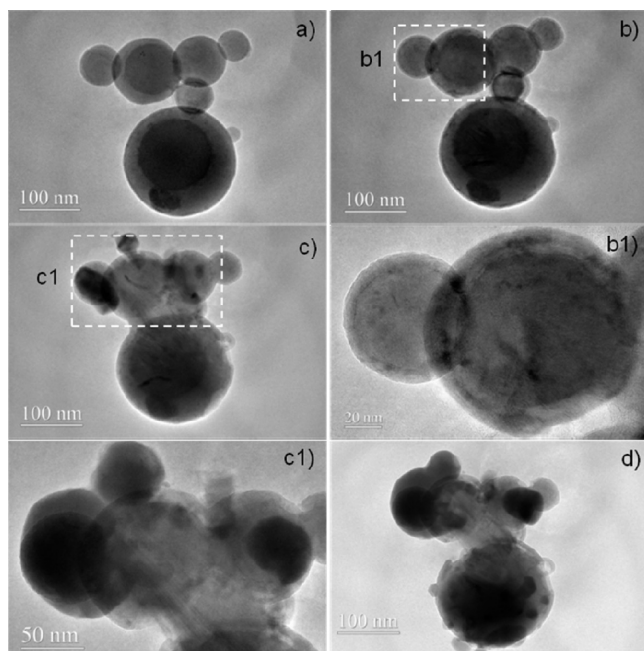


Figure 8. Hot-stage TEM images of aluminum nanoparticles obtained at (a) 300 °C, (b) 600 °C, (c) 750 °C, and (d) 750 °C 15 min after taking (c). (b1) and (c1) magnify the dotted regions in (b) and (c), respectively.

amorphous–crystalline interface or significant dislocation) that were preferentially fractured. Last, we would like to emphasize that our speculation about the localized partial crystalline transformation is exactly evidenced by Figure 7b1.

In situ observation using hot-stage TEM has been made to trace the overall morphology change of the Alex sample, regarding the shell thickening. While ramping the temperature, a group of spherical particles were chosen, and their image was captured at 300, 600, and 750 °C as seen in Figure 8a–c, respectively. After holding the temperature of the sample in Figure 8c for about 15 min, another image was again taken, and shown in Figure 8d. Two spherical particles are hidden by the bigger spheres in Figure 8a (on top of or underneath the bottom one and the second left one). This overall shape maintains until 600 °C as seen in Figure 8b. When the temperature reaches 750 °C, the major part of the second left sphere obviously melts and liquid Al flows out. In addition, a new small sphere appears from the second left one. After 15 min, significant changes are observed throughout all particles except the top right sphere. The magnified image Figure 8b1 of Figure 8b indicates a significant thickening of the shell even at the highest vacuum condition, which is again consistent with the findings from Figures 6 and 7.

4. CONCLUSIONS

In this study, microstructural behaviors of Al core and alumina shell lattices have been investigated with increasing temperatures. High-temperature X-ray diffraction analysis revealed that nano aluminum lattice was initially expanded under tension at room temperature, and then when heated passed through a zero-strain state \sim 300 °C. Upon further heating above the bulk melting temperature of aluminum, the aluminum lattice expanded under almost no constraint. This interesting observation, which is contrary to almost all of the previous results and models, was ascribed to the inhomogeneous (localized) crystalline phase

transformation of amorphous alumina. High-resolution transmission electron microscopy and in situ hot-stage transmission electron microscopy evidenced localized phase transformation accompanied by a significant shell thickening, presumably resulting from diffusion processes of Al cations and O anions, which is to absorb the pressure built in the aluminum core, by creating a more ductile shell.

AUTHOR INFORMATION

Corresponding Author

*E-mail: donglee@pusan.ac.kr (D.L.), mrz@umd.edu (M.R.Z.).

ACKNOWLEDGMENT

This work was supported by the National Research Foundation of Korea (NRF) grants funded by the Korean government (MEST) (No. 2011-0027954 and No. 2011-0027562). M.R.Z. and K.S. were supported by the Army Research Office.

REFERENCES

- (1) Brousseau, P.; Anderson, C. J. *Propellants, Explos., Pyrotech.* **2002**, *27*, 300.
- (2) Levitas, V. I.; Asay, B. W.; Son, F. S.; Pantoya, M. L. *J. Appl. Phys.* **2007**, *101*, 083524.
- (3) Ivanov, G. V.; Tepper, F. In *Challenges in Propellants and Combustion - 100 Years After Nobel*; Kuo, K. K., et al., Eds.; Begell House: New York, 1997; p 636.
- (4) Moore, K.; Pantoya, M. L. *J. Propul. Power* **2007**, *23*, 1.
- (5) Sun, J.; Pantoya, M. L.; Simon, S. L. *Thermochim. Acta* **2006**, *444*, 117.
- (6) Trunov, M. A.; Schoenitz, M.; Dreizin, E. L. *Combust. Theory Modell.* **2006**, *10*, 603. Trunov, M. A.; Schoenitz, M.; Dreizin, E. L. *Propellants, Explos., Pyrotech.* **2005**, *40*, 36.
- (7) Trunov, M. A.; Umbrajkar, S. M.; Schoenitz, M.; Mang, J. T.; Dreizin, E. L. *J. Phys. Chem. B* **2006**, *110*, 13094.
- (8) Park, K.; Lee, D.; Rai, A.; Mukherjee, D.; Zachariah, M. R. *J. Phys. Chem. B* **2005**, *109*, 7290.
- (9) Chowdhury, S.; Sullivan, K.; Piekielek, N.; Zhou, L.; Zachariah, M. R. *J. Phys. Chem. C* **2010**, *114*, 9191.
- (10) Levitas, V. I.; Asay, B. W.; Son, S. F.; Pantoya, M. *J. Appl. Phys. Lett.* **2006**, *89*, 071909.
- (11) Levitas, V. I.; Asay, B. W.; Son, S. F.; Pantoya, M. *J. Appl. Phys.* **2007**, *101*, 083524.
- (12) Levitas, V. I.; Pantoya, M.; Dikici, B. *J. Appl. Phys. Lett.* **2008**, *92*, 011921.
- (13) Levitas, V. I.; Pantoya, M. L.; Chauhan, G.; Rivero, I. *J. Phys. Chem. C* **2009**, *113*, 14088.
- (14) Henz, B. J.; Hawa, T.; Zachariah, M. R. *J. Appl. Phys.* **2010**, *107*, 024901.
- (15) Mei, Q. S.; Wang, S. C.; Cong, H. T.; Jin, Z. H.; Lu, K. *Acta Mater.* **2005**, *53*, 1059.
- (16) Sun, J.; Simon, S. L. *Thermochim. Acta* **2007**, *463*, 32.
- (17) Rufino, B.; Coulet, M.-V.; Bouchet, R.; Isnard, O.; Denoyel, R. *Acta Mater.* **2010**, *58*, 4224.
- (18) Choi, I. D.; Lee, H.; Shim, Y.-B.; Lee, D. *Langmuir* **2010**, *26*, 11212.
- (19) Kim, Y. H.; Kim, Y.-T.; Kim, S. H.; Lee, D. *Carbon* **2010**, *48*, 2072.
- (20) Wu, C.; Lee, D.; Zachariah, M. R. *Langmuir* **2010**, *26*, 4327.
- (21) Firmansyah, D. A.; Kim, T.; Kim, S.; Sullivan, K.; Zachariah, M. R.; Lee, D. *Langmuir* **2009**, *25*, 7063.
- (22) Rozita, Y.; Brydson, R.; Scott, A. J. *J. Phys.: Conf. Ser.* **2010**, *241*, 012096.
- (23) Damani, R. J.; Mackroczy, P. *J. Eur. Ceram. Soc.* **2000**, *20*, 867.

- (24) De Weijer, A. P.; Lucasius, C. B.; Buydens, L.; Kateman, G. *Anal. Chem.* **1994**, *66*, 23.
- (25) Kang, S. K.; Jeong, S. M.; Kim, S. D. *Ind. Eng. Chem. Res.* **2000**, *39*, 2496.
- (26) Campbell, T.; Kalia, R. K.; Nakano, A.; Vashishta, P. *Phys. Rev. Lett.* **1999**, *82*, 4866.